

OMAE2005-67075

## A COUPLED-MODE, PHASE-RESOLVING MODEL FOR THE TRANSFORMATION OF WAVE SPECTRUM OVER STEEP 3D TOPOGRAPHY. A PARALLEL-ARCHITECTURE IMPLEMENTATION

Th.P. Gerothathis, K. A. Belibassakis and G.A. Athanassoulis

School of Naval Architecture and Marine Engineering  
National Technical University of Athens  
Zografos 15773, Athens, GREECE

### ABSTRACT

The problem of transformation of the directional spectrum of an incident wave system over a region of strongly varying three-dimensional bottom topography is studied, in the context of linear theory. The Consistent Coupled-Mode Model (Athanassoulis and Belibassakis 1999, Belibassakis *et al* 2001) is exploited for the calculation of the linear transfer function, connecting the incident wave with the wave conditions at each point in the field. This model takes fully into account reflection, refraction and diffraction phenomena. The present approach permits the consistent transformation of any incident directional wave spectrum over a variable bathymetry region and the calculation of the spatial evolution of point spectra of all interesting wave quantities (free surface elevation, velocity, pressure), at every point in the domain. This approach can be extended to treat weakly non-linear waves.

### 1. INTRODUCTION

In this work, the problem of transformation of the directional spectrum of an incident wave system over a region of strongly varying three-dimensional bottom topography is studied, in the context of linear theory.

The keystone of the present approach lies on the utilization of the Consistent Coupled-Mode Model (CCMM), developed by Athanassoulis and Belibassakis (1999) and generalised to 3D by Belibassakis *et al* (2001), for the consistent calculation of the corresponding deterministic wave field, for each frequency, through which the transfer functions between any two (possibly different) physical quantities of interest, at any two points in the variable bathymetry domain are obtained. The main features of CCMM are: (a) the exact calculation of the wave field (velocity and pressure field up to and including the bottom boundary), without any assumption on the bottom slope and curvature, and

(b) its ability to reduce to simplified one-equation models, such as the modified mild-slope equation (Massel, 1993, Chamberlain and Porter, 1995), at subregions where such a simplification is permitted

The application of CCMM to realistic geographical domains requires a vast amount of calculations. In this work, a parallel implementation of CCMM is presented using Message Passing Interface. Numerical results obtained by the present model are compared with observations of surface wave transformation over the Scripps Canyon, collected during the NSF/ONR NCEX experiment.

The present approach provides us with a tool enabling the description of the stochastic characteristics of all important physical quantities associated with the wave field (induced wave kinematics), taking fully into account the diffraction effects. The present model can be further elaborated for modeling and studying wave propagation over random bottom topography, e.g. in the line of works by Pelinovsky *et al.* (1998), Ardhuin and Herbers (2002).

Although our present approach is based on the framework of linear theory, it still brings into light significant features as concerns the effects of seabed steepness and 3D bottom effects. Based on already developed extensions of the deterministic CCMM, the present approach can also be extended to treat the resulting second-order refraction-diffraction patterns, with application to the transformation of second-order random seas in variable bathymetry regions. Second-order effects can be incorporated by means of the corresponding quadratic transfer functions, exploiting the work by Belibassakis and Athanassoulis (2002) extending the deterministic CCMM to second-order Stokes waves in variable bathymetry regions.

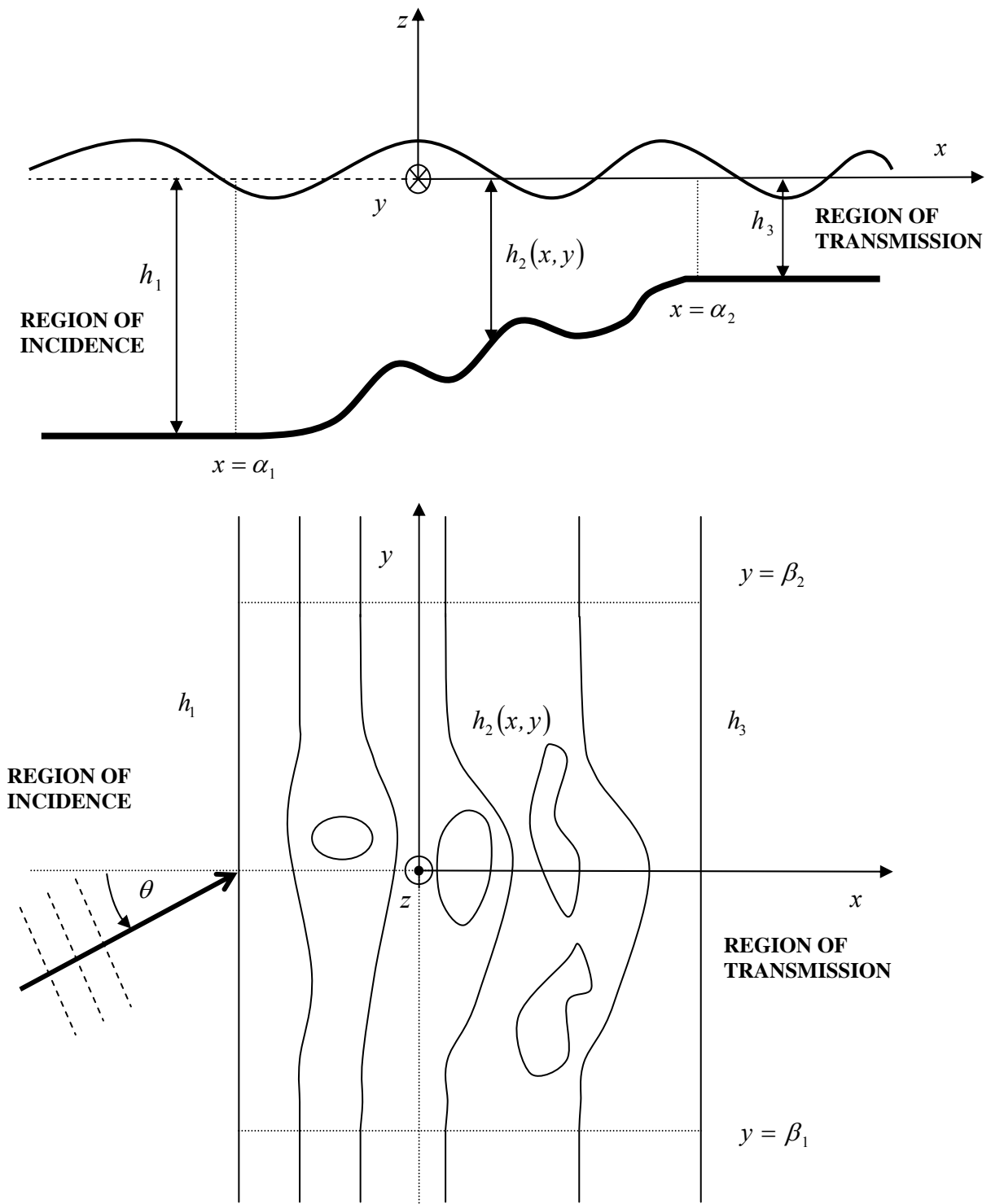


Figure 1. Irregular water waves propagating over a variable bathymetry region. Basic notation

## 2. DESCRIPTION OF THE ENVIRONMENT

We consider irregular wave propagation in a variable bathymetry region. The liquid is assumed inviscid and the flow irrotational. The forcing of the system comes from an incident wave system generated in the far up-wave region ( $x \rightarrow -\infty$ ), which is completely defined by the corresponding incident directional wave spectrum  $S_{INC}(\omega, \theta)$ ; see Fig.1.

We consider a fixed (deterministic) bottom topography and no other free-surface forcing attributes, as e.g., wind-input, and thus, the random character of the wave field is induced only by the incident wave system. Under the additional assumption of waves of small steepness, small-amplitude (linear) wave theory can be used. We introduce however, no assumption as regards the mildness of the bottom surface. The essential features of the random wave field in this case are strong spatial

inhomogeneity combined with pointwise stationarity at any given point in the wave field.

A Cartesian coordinate system is used having its origin at some point on the unperturbed free-surface ( $z = 0$ ). The  $z$ -axis is pointing upwards and the  $x$ -axis is pointing along the direction of the transmitted wave field; see Fig. 1. The incident wave conditions are represented by the frequency spectrum  $S_{INC}(\omega, \theta)$ . Given the incident wave spectrum, the (free-surface elevation) spectra  $S(\omega; x, y)$ , at each point  $(x, y)$  of the horizontal plane, can be obtained as

$$S(\omega; x, y) = \int_{-\pi/2}^{\pi/2} S_{INC}(\omega, \theta) \cdot |K(\omega, \theta; x, y)|^2 d\theta, \quad (2.1)$$

where  $K(\omega, \theta; x, y)$  denotes the appropriate transfer function associated with the harmonic wave solution in the area, corresponding to a given incident wave frequency  $\omega$  and direction  $\theta$ ; see, e.g., Goda (2000). The spectra associated with other physical quantities can be similarly obtained through the appropriate transfer functions.

In order to obtain the complete harmonic wave solutions and the transfer function, in this work, the depth  $h(x, y)$  is decomposed as follows:

$$h(x, y) = h_i(x) + h_d(x, y), \quad (2.2)$$

where  $h_i(x)$  represents a parallel-contour surface and  $h_d(x, y)$  a perturbation bottom topography. The parallel-contour topography  $h_i(x)$  is defined as

$$h_i(x) = \max_y \{h(x, y)\}, \quad (2.3)$$

and the scattering bottom topography as

$$h_d(x, y) = h(x, y) - h_i(x). \quad (2.4)$$

The 3D harmonic wave solution is then obtained as the linear superposition of the wave field excited by the obliquely incident harmonic waves over the background 2D topography  $h_i(x)$  and the 3D scattering potential induced by the perturbation bathymetry  $h_d(x, y)$ , as explained below.

### 3. THE DETERMINISTIC CCMM

Considering the velocity field to be time harmonic, its angular frequency  $\omega$  and direction  $\theta$  being the same with the corresponding component of the incident wave system, the flow field is described by a velocity potential of the form

$$\Phi(x, y, z; t) = \text{Re} \left\{ -\frac{igH}{2\omega} \phi(x, y, z; \mu) \exp(-i\omega t) \right\}, \quad (3.1)$$

where  $g$  is the acceleration due to gravity,  $\mu = \omega^2 / g$  is the frequency parameter,  $H$  is the oblique-incident wave height and  $i = \sqrt{-1}$ . The function  $\phi = \phi(x, y, z; \mu)$  is the normalized potential in the frequency domain, usually written as  $\phi(x, y, z)$ .

Under the previous assumptions  $\phi(x, y, z)$  satisfies:

$$\left( \frac{\partial^2}{\partial z^2} + \nabla^2 \right) \phi(x, y, z) = 0, \quad (3.2a)$$

$$\frac{\partial \phi}{\partial z} - \mu \phi = 0, \quad z = 0, \quad (3.2b)$$

$$\left( \frac{\partial}{\partial z} + \nabla h \nabla \right) \phi = 0, \quad z = -h(x, y), \quad (3.2c)$$

where  $\nabla = \left( \frac{\partial}{\partial x}, \frac{\partial}{\partial y} \right)$  is the horizontal gradient operator. The

above problem is forced by the oblique-incident wave, characterized by the potential

$$\exp\left( i(\kappa_x x + \kappa_y y) \right) \frac{\cosh\left( k_0^{(1)}(z + h_1) \right)}{\cosh\left( k_0^{(1)} h_1 \right)}. \quad (3.3)$$

The wavenumber vector of the oblique-incident wave is

$$(\kappa_x, \kappa_y) = k_0^{(1)} (\cos \theta, \sin \theta), \quad (3.4)$$

where  $k_0^{(1)}$  is the positive root of the dispersion relation  $\mu h_1 = k_0^{(1)} h_1 \tanh\left( k_0^{(1)} h_1 \right)$  in the region of incidence.

Exploiting the linearity of the problem (3.2) and the depth definition (2.2), the total wave potential  $\phi(x, y, z)$  can be decomposed in two parts: (i) the potential  $\phi_i(x, y, z)$  representing the propagation over the parallel-contour surface  $h_i(x)$ , which will be called the *incident wave field*, and (ii) the potential  $\phi_d(x, y, z)$  representing the *diffraction field* by the 3D bathymetric features  $h_d(x, y)$ ,

$$\phi(x, y, z) = \phi_i(x, y, z) + \phi_d(x, y, z). \quad (3.5)$$

Based on physical grounds we assume that, since the oblique-incident wave (3.3) is periodic along the  $y$ -direction, the incident potential  $\phi_i(x, y, z)$  is also  $y$ -periodic with the same wavelength  $\lambda = 2\pi / \kappa_y$ , where  $\kappa_y = k_0^{(1)} \sin \theta$ ; see, e.g., Massel (1993). Thus, by introducing the factorisation

$$\phi_i(x, y, z) = e^{i\kappa_y y} \varphi_i(x, z), \quad (3.6)$$

we obtain the following 2D problem for  $\varphi_i(x, z)$ :

$$\frac{\partial^2 \varphi_i(x, z)}{\partial x^2} + \frac{\partial^2 \varphi_i(x, z)}{\partial z^2} - \kappa_y^2 \varphi_i(x, z) = 0, \quad (3.7a)$$

$$\frac{\partial \varphi_i(x, z)}{\partial z} - \mu \varphi_i(x, z) = 0, \quad z = 0, \quad (3.7b)$$

$$\left( \frac{\partial}{\partial z} + \frac{dh_i}{dx} \frac{\partial}{\partial x} \right) \varphi_i(x, z) = 0, \quad z = -h_i(x), \quad (3.7c)$$

supplemented by the radiation conditions

$$\varphi_i(x, z) \sim \left[ e^{ik_0^{(1)} \cos \theta_i x} + A_R e^{-ik_0^{(1)} \cos \theta_i x} \right] \frac{\cosh\left( k_0^{(1)}(z + h_1) \right)}{\cosh\left( k_0^{(1)} h_1 \right)}, \quad (3.8d)$$

$$x \rightarrow -\infty,$$

$$\varphi_i(x, z) \sim A_T e^{ik_0^{(3)} \cos \theta_3 x} \frac{\cosh(k_0^{(3)}(z+h_3))}{\cosh(k_0^{(3)}h_3)}, \quad x \rightarrow +\infty. \quad (3.8e)$$

In the above equations,  $A_R$  and  $A_T$  are reflection and transmission coefficients, respectively. The direction of the wave in the region of transmission is given by

$$\theta_3 = \sin^{-1}(k_0^{(1)} \sin \theta_1 / k_0^{(3)}), \quad (3.9)$$

and the wavenumbers  $k_0^{(m)}$ ,  $m=1,3$ , in the regions of incidence and transmission, appearing in Eqs. (3.8) are obtained by the corresponding dispersion relations

$$\mu h_m = k_0^{(m)} h_1 \tanh(k_0^{(m)} h_m), \quad m=1,3, \quad (3.10)$$

formulated at the depths  $h_m$ ,  $m=1,3$ , respectively.

By substituting the decomposition (3.5) in Eqs. (3.2) and using Eqs. (3.7) and (3.8), we finally obtain the following problem concerning the diffraction potential  $\phi_d(x, y, z)$ :

$$\left( \frac{\partial^2}{\partial z^2} + \nabla^2 \right) \phi_d(x, y, z) = 0, \quad (3.11a)$$

$$\frac{\partial \phi_d}{\partial z} - \mu \phi_d = 0, \quad z=0, \quad (3.11b)$$

$$\left( \frac{\partial}{\partial z} + \nabla h \nabla \right) \phi_d = - \left( \frac{\partial}{\partial z} + \nabla h \nabla \right) \phi_i, \quad z=-h(x, y) \quad (3.11c)$$

supplemented by the radiation condition requiring that

$$\phi_d \sim \text{outgoing waves as } R = \sqrt{x^2 + y^2} \rightarrow \infty. \quad (3.11d)$$

The support of the forcing  $g(x, y) = - \left( \frac{\partial}{\partial z} + \nabla h \nabla \right) \phi_i$  of diffraction problem (3.11) is exactly the same as the support of the localized scatterer(s)  $h_d(x, y)$ .

The wave potentials  $\varphi_i(x, z)$  and  $\phi_d(x, y, z)$  associated with the propagation/diffraction of water waves over the background parallel-contour bathymetry and the scattering bottom topography, respectively, are treated by means of the consistent coupled-mode model (CCMM) developed by Athanassoulis & Belibassakis (1999) and extended to 3D by Belibassakis *et al* (2001). This model is based on the following *enhanced local-mode representation* of the generalised incident wave potential:

$$\varphi_i(x, z) = \varphi_{-1}(x) Z_{-1}(z; x) + \varphi_0(x) Z_0(z; x) + \sum_{n=1}^{\infty} \varphi_n(x) Z_n(z; x) \quad (3.12)$$

and similar expression for the scattering potential  $\phi_d(x, y, z)$ .

In the above expansion, the term  $\varphi_0(x) Z_0(z; x)$  denotes the *propagating mode* of the generalised incident field. The remaining terms  $\varphi_n(x) Z_n(z; x)$ ,  $n=1,2,\dots$ , are the *evanescent modes* and the additional term  $\varphi_{-1}(x) Z_{-1}(z; x)$  is a correction term, called the *sloping-bottom mode*, which properly accounts

for the satisfaction of the Neumann bottom boundary condition on the non-horizontal parts of the bottom. The function  $Z_n(z; x)$  represents the vertical structure of the  $n$ -th mode. The *complex amplitude*  $\varphi_n(x)$  describes the horizontal pattern of the  $n$ -th mode. The functions  $Z_n(z; x)$ ,  $n=0,1,2,\dots$ , appearing in Eq. (3.12) are obtained as the eigenfunctions of local vertical *Sturm-Liouville* problems, and are given by

$$Z_0(z; x) = \frac{\cosh[k_0(z+h)]}{\cosh(k_0 h)}, \quad (3.13a)$$

$$Z_n(z; x) = \frac{\cos[k_n(z+h)]}{\cos(k_n h)}, \quad n=1,2,\dots, \quad (3.13b)$$

where the eigenvalues  $\{ik_0, k_n\}$  are obtained as the roots of the dispersion relation

$$\mu h = -k h \tan(kh), \quad a \leq x \leq b, \quad (3.13c)$$

formulated at the local depth. A specific convenient form of the function  $Z_{-1}(z; x)$  is given by

$$Z_{-1}(z; x) = h \left( (z/h)^3 + (z/h)^2 \right), \quad (3.14)$$

and all numerical results presented in this work are based on this choice for  $Z_{-1}(z; y)$ . However, other choices are also possible; see Athanassoulis & Belibassakis (1999, Sec.4).

An important feature of the calculation of the incident and diffraction fields by means of the enhanced representation, is that it exhibits an improved rate of decay of the modal amplitudes  $|\varphi_n|$  of the order  $O(n^{-4})$ . Thus, only a few number of modes suffice to obtain a convergent solution, even for bottom slopes above 100%. In addition, if only the propagating mode  $\varphi_0(x)$  is retained in the local-mode series, the present coupled-mode system exactly reduces to the simplified Modified Mild-Slope model (MMS) developed by Massel (1993) and Chamberlain & Porter (1995).

The resulting coupled-mode systems of equations for each one of the unknown potentials  $\varphi_i(x, z)$  and  $\phi_d(x, y, z)$  are discretized using finite differences. Details about the numerical implementation of the present method, as well as comparisons of present method results with other models and experimental data can be found in Athanassoulis & Belibassakis (1999), and as concerns its application to 3D seabed topographies in Belibassakis *et al* (2001).

#### 4. TRANSFER FUNCTION AND STOCHASTIC OUTPUT

Having calculated the complex wave potential  $\Phi(x, y, z)$  for each single frequency  $\omega$  and direction  $\theta$ , as provided by the solution of CCMM, the complex amplitude of any other physical quantity of interest, at every point in the domain, can be easily calculated. For example, the free-surface elevation is obtained by

$$\eta(x, y; \omega, \theta) = \frac{i\omega}{g} \Phi(x, y, z=0; \omega, \theta), \quad (4.1)$$

the horizontal and vertical wave velocity components by

$$\vec{u}(x, y, z; \omega, \theta) = \nabla_{3D} \Phi(x, y, z; \omega, \theta), \quad (4.2)$$

where  $\nabla_{3D} = \left( \frac{\partial}{\partial x}, \frac{\partial}{\partial y}, \frac{\partial}{\partial z} \right)$  is the 3D gradient operator, and the (dynamic) pressure by

$$p(x, y, z; \omega, \theta) / \rho = i\omega \Phi(x, y, z=0; \omega, \theta), \quad (4.3)$$

where  $\rho$  denotes the fluid density. Then, on the basis of linear system theory applied to our distributed system, the transfer function between any two quantities at any two points is obtained as the ratio of the corresponding complex amplitudes. For example, the transfer function between anyone of the above quantities (compactly denoted as  $M$ ) and the free-surface elevation associated with the incident wave system is

$$K(\omega, \theta; x, y, z) = \frac{M(x, y, z; \omega, \theta)}{H(\omega) / 2}. \quad (4.4)$$

In this way, the spatial distribution of the spectrum associated with each quantity  $M$ , is expressed as

$$S_M(\omega; x, y, z) = \int_{-\pi/2}^{\pi/2} S_{INC}(\omega, \theta) |K(\omega, \theta; x, y, z)|^2 d\theta, \quad (4.5)$$

and its moments are obtained by frequency integration,

$$m_v(x, y, z) = \int_0^{+\infty} \omega^v S_M(\omega; x, z) d\omega, \quad v=0,1,2,\dots \quad (4.6)$$

## 5. PARALLEL ARCHITECTURE IMPLEMENTATION

The computation cost associated with the calculation of the transfer functions for all combinations of frequencies and directions involved in the incident wave spectrum is huge, especially if we take into account that in real applications the horizontal dimensions of the physical domain are large, usually of the order of several kilometers.

In order to efficiently implement the present method a parallel code is build using message passing paradigm, open source compilers and libraries, and tested on a commodity computer cluster. This programming model and hardware architecture has been selected because of its great portability, low cost of implementation in comparison with the performance and great scalability. In order to maximize the portability of the code, the model is implemented using ANSIC++ programming language and the Message Passing Interface (MPI) standard.

The concurrency of the calculations has been achieved by:

- i. the separation of the problems to different frequencies/directions
- ii. the decomposition of the resulting very large systems of equations with complex coefficients.

The two fields  $\phi_i(x, z)$  and  $\phi_d(x, y, z)$  composing the total deterministic wave field for each different frequency/direction are sequentially calculated. First the incident wave potential  $\phi_i(x, z)$  is calculated. Then, the forcing  $g(x, y)$  is evaluated

and finally the diffraction potential  $\phi_d(x, y, z)$  is calculated.

Each part of the above calculations is performed in parallel, on the basis of the decomposition of the computational domain in as many parts as the number of processes used. Each process is executed on a different computer node that communicates with the others for exchanging results through messages.

The resulting very large sparse systems of equations are solved using distributed direct and iterative solvers. In the realization of the present code PETSc (Balay *et al* 2003) and SuperLU (Demmel *et al* 1999) libraries have been used. These libraries are open-source, well-tested and can be compiled on different architectures. Numerical results have been obtained using a computer cluster consisted of nine PC nodes. The hardware configuration of each node contains one Pentium 4 CPU at 2.8 GHz, 1 Gb memory and gigabit Ethernet. The nodes are interconnected with a Gigabit switch.

## 6. NUMERICAL RESULTS AND DISCUSSION

As an example, we consider the steep topography of Scripps and La Jolla submarine canyons in Southern California, Fig. 2. This bottom topography produces dramatic changes in wave energy over alongshore distances of only a few hundred meters, resulting in complex nearshore circulation and morphological changes. Aiming to investigate how this complex bathymetry affects nearshore processes such as wave evolution, swash zone dynamics, nearshore circulation, the Nearshore Canyon EXperiment (<http://science.whoi.edu/users/elgar/NCEX/>) is running, following a number of experiments carried out at the U.S. Army Corps of Engineers Field Research Facility in a region of gently sloping bathymetry.

Offshore wave conditions in this area typically consist of Western – North Western swell systems with peak periods ranging from 10-22 sec. In order to investigate the effects of steep 3D topography on nearshore wave refraction and diffraction phenomena, we consider a test case corresponding to a western swell characterised by mean wave (peak) period  $T_p = 15$ sec and significant wave height of  $H_s = 1$ m; see Fig.3.

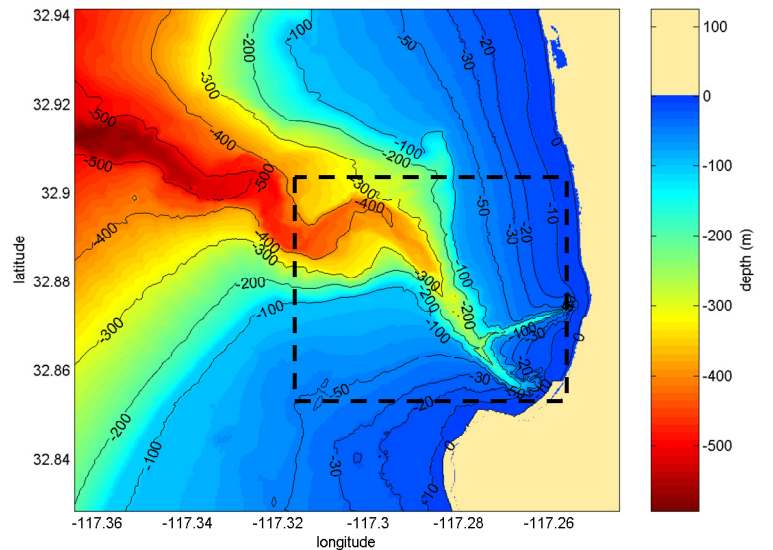


Fig. 2. The steep 3D topography of Scripps and La Jolla submarine canyons in Southern California. The computational domain used for the calculation of the transformation of the offshore spectrum is shown by means of a dashed rectangle.

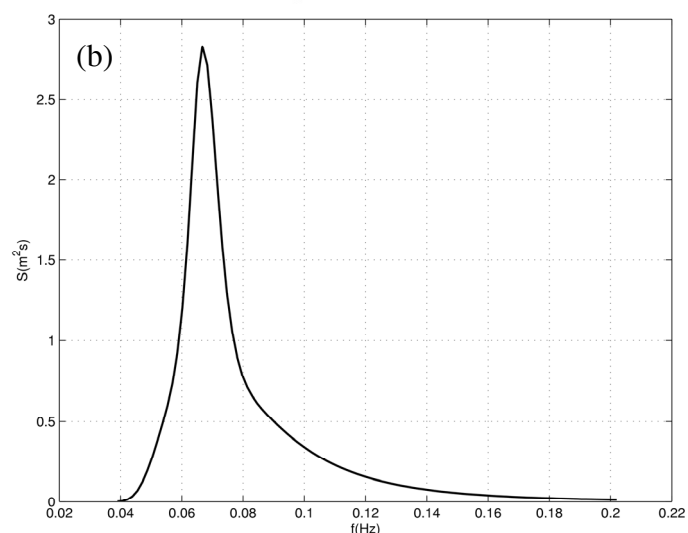
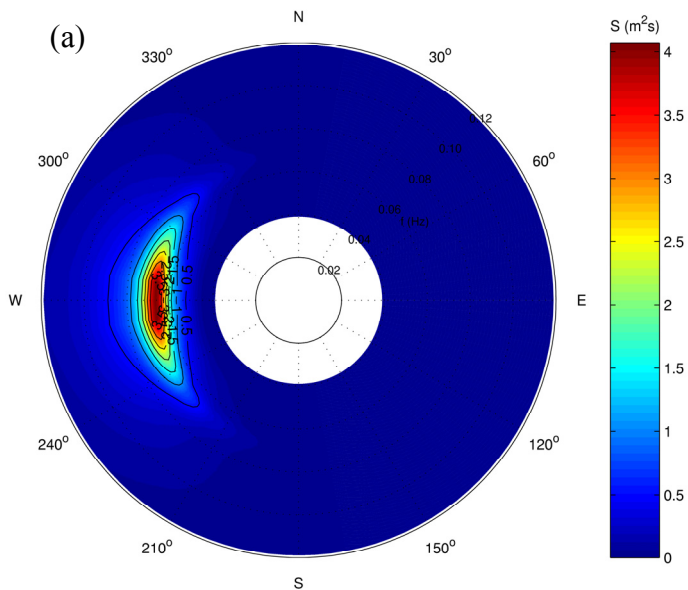


Fig. 3. (a) The directional and (b) the frequency spectrum corresponding to a western swell system, characterised by  $H_s = 1m, T_p = 15s$ .

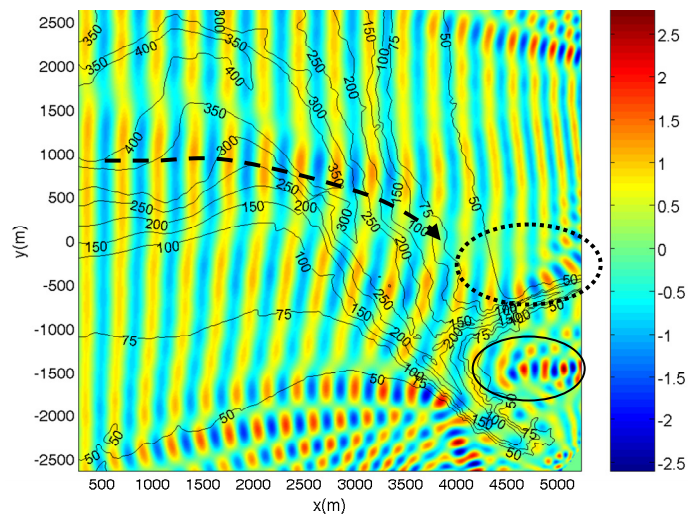


Fig. 4. The total wave field on the free surface (real part) excited by a harmonic obliquely incident wave of period  $T=15s$  coming from the west ( $\theta=0deg$ ).

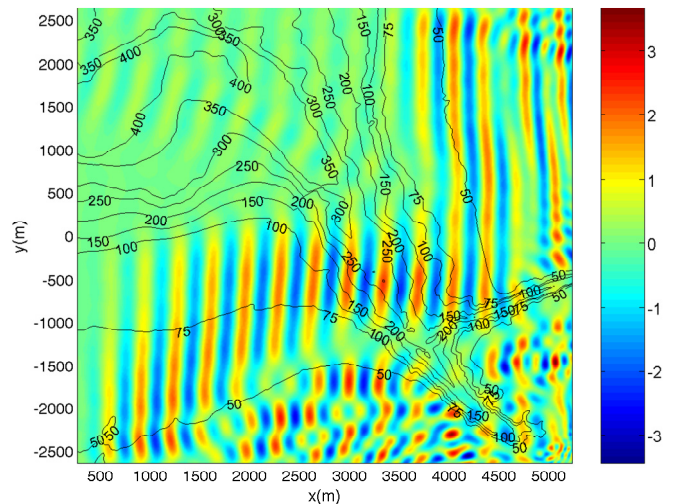


Fig. 5. Real part of the propagating mode ( $n=0$ ) of the scattering wave potential corresponding to incident wave of period  $T=15s$  coming from the west ( $\theta=0deg$ ).

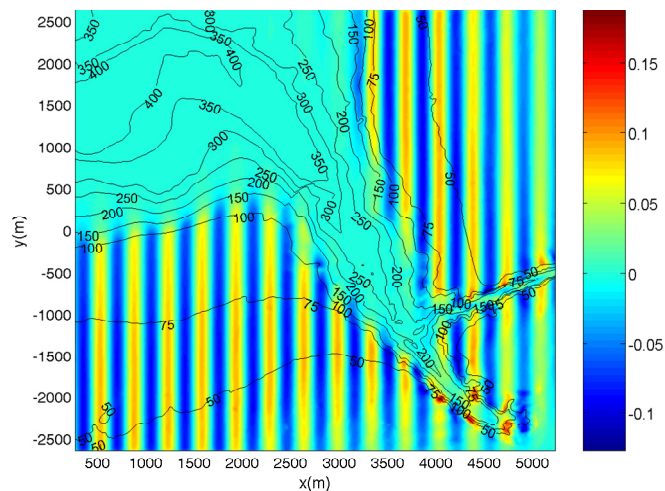


Fig. 6. Real part of the first evanescent mode ( $n=1$ ) of the scattering wave potential corresponding to incident wave of period  $T=15s$  coming from the west ( $\theta=0deg$ ).

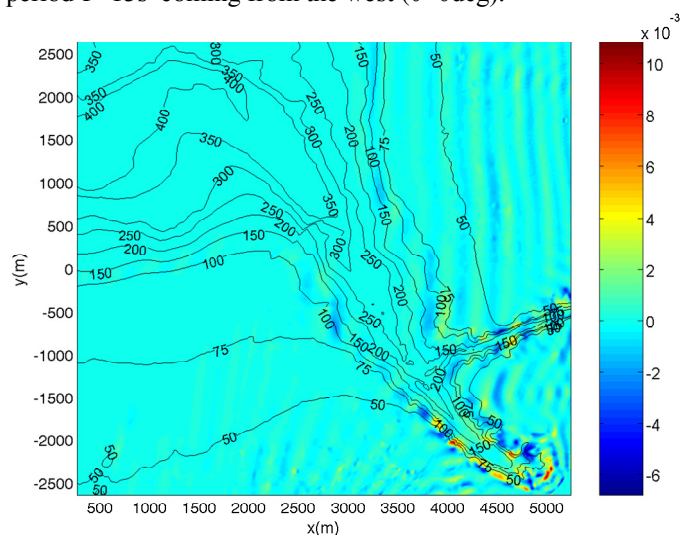


Fig. 7. Real part of the sloping-bottom mode ( $n=-1$ ) of the scattering wave potential corresponding to incident wave of period  $T=15s$  coming from the west ( $\theta=0deg$ ).

The offshore directional wave spectrum has been reconstructed from integrated wave parameters by using a standard JONSWAP frequency spectrum, in conjunction with a hyperbolic cosine-type directional spreading function (Donelan *et al* 1985), defined as follows

$$D(\theta; \Theta) = \frac{1}{2} \beta \cosh^{-2} [\beta(\theta - \Theta)], \quad (6.1)$$

where

$$\beta = \begin{cases} 2.61(\omega/\omega_p)^{1.3}, & \text{for } 0.562 < \omega/\omega_p < 0.95 \\ 2.28(\omega/\omega_p)^{-1.3}, & \text{for } 0.95 \leq \omega/\omega_p < 1.60 \\ 1.24, & \text{otherwise} \end{cases}, \quad (6.2)$$

where  $\omega_p = 2\pi/T_p$  and  $\Theta$  stands for the mean wave direction; see also Massel (1996).

The directional and the frequency incident spectra corresponding to a typical western swell in the NCEX area, characterised by  $H_s = 1m, T_p = 15s$ , which is used for wave calculations are shown in Fig. 3. In Fig.4, we present the calculated wave pattern associated with the real part of the total wave field  $\phi(x, y, z) = \phi_i(x, y, z) + \phi_d(x, y, z)$ , on the free surface ( $z=0$ ), as obtained through the solution of the present CCMM, using the first three modes ( $n=-1,0,1$ ) and 501X501 gridpoints to discretize the physical domain (on the horizontal plane). The solution shown corresponds to the harmonic wave field excited by an obliquely incident wave of period  $T=15s$  (equal to the peak spectral period) coming from the west ( $\theta=0deg$ ).

We are able to observe in this figure the main effects of refraction on this particular wave component, indicated by using a dotted arrow, as well as the effects of strong reflection and diffraction induced by the nearshore canyon tips, which are depicted in the colorplot as the encircled subareas by using dotted and solid lines, respectively.

Aiming to illustrate the significance of the most important modes, in Figs. 5, 6 and 7 the real parts of the propagating mode  $\varphi_0(x, y)$ , the first evanescent mode  $\varphi_1(x, y)$  and the sloping-bottom mode  $\varphi_{-1}(x, y)$ , respectively, associated with the scattering potential  $\phi_d(x, y, z)$ , are plotted. We observe in these figures that the main effects of wave refraction and diffraction are carried out by the propagating mode. This fact justifies the use of the simplified, one-equation MMS model to obtain approximate results. However, as shown by Athanassoulis *et al* (2003), the applicability of the latter model is restricted to slowly varying bottom topographies.

Moreover, in Fig.6 we observe that the first evanescent mode  $\varphi_1(x, y)$  is one order of magnitude less than the propagating mode. This mode is clearly connected with the disturbance bathymetry  $h_d(x, y)$  and the forcing  $g(x, y)$  of the diffraction subproblem. Furthermore, the sloping-bottom mode  $\varphi_{-1}(x, y)$  is one order of magnitude less than the first evanescent mode. As clearly shown in Fig. 7, this mode is localized in the areas

of strong gradients of the real bathymetry  $h(x, y)$ , having essential support at the places where the canyon walls become nearly vertical.

In Figs. 8 and 9 we present a comparison concerning the spatial distribution of the significant wave height  $H_s$  over the computational domain for the incident spectrum of Fig.3. Results obtained by the present method, in conjunction with systematic application of Eq. (5.6) for the zero moment ( $H_s = 4\sqrt{m_0}$ ) of the free-surface elevation spectra at each gridpoint  $(x, y)$ , are shown in Fig. 8. The application of the third-generation SWAN (ver. 40.41) model, Booij *et al* (1999), Ris *et al* (1999), is shown in Fig. 9. One important feature of this (current) version of SWAN is the incorporation of diffraction effects, Holthuijsen *et al* (2003). For compatibility in the comparison, bottom friction and (nearshore) wave breaking processes in SWAN have been turned off. The agreement between the present method and SWAN results is generally good, showing that the latter model in its current version is able to predict strong 3D diffraction effects. Still,

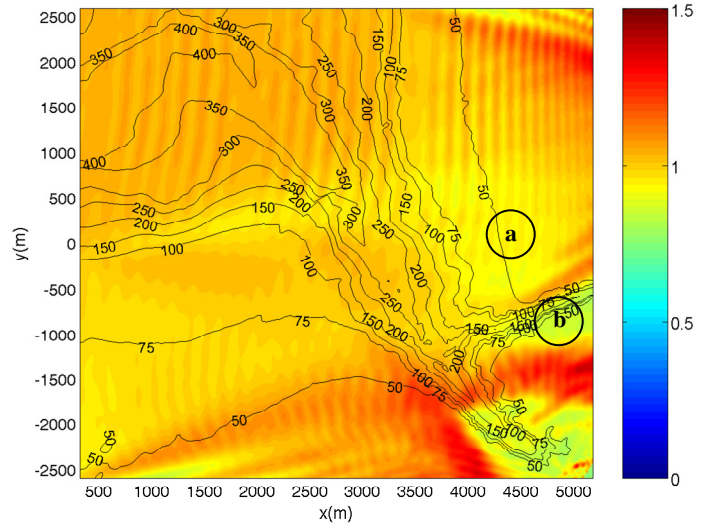


Fig.8 Distribution of the significant wave height  $H_s$  in the NCEX, as obtained by the present method.

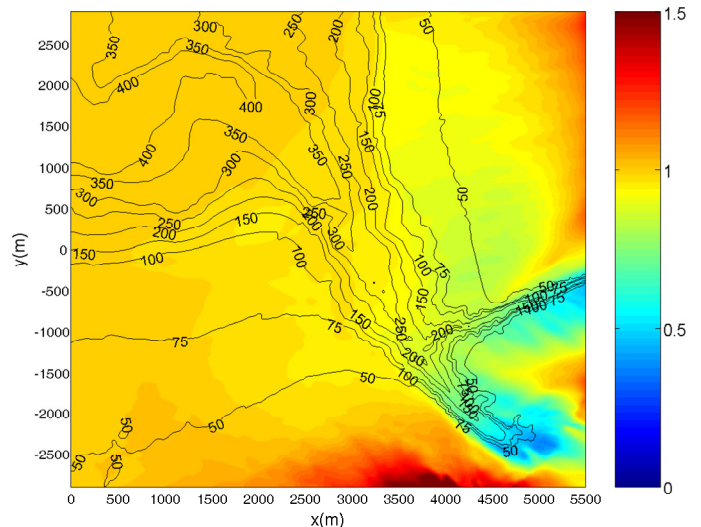


Fig.9 Distribution of the significant wave height  $H_s$  in the NCEX area, as obtained by SWAN.

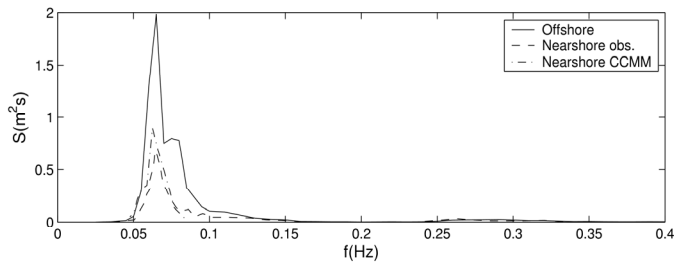


Fig.10 Calculated and observed spectra at point (a).

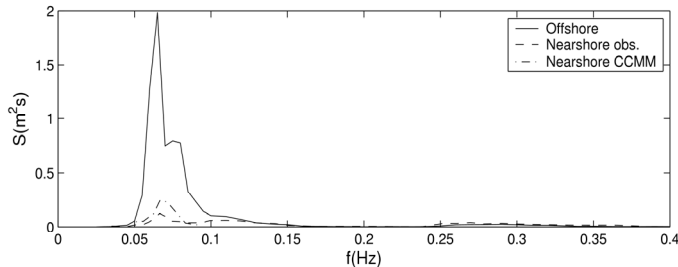


Fig.11 Calculated and observed spectra at point (b).

however there remain some notable differences at the shallow canyon tips, where SWAN seems to underestimate the waveheight.

Finally, for an observed offshore swell system, incident from the west in the NCEX area, characterised by  $H_s = 0.77m, T_p = 15.3s$ , we present in Figs. 11 and 12, comparisons between the present model results and buoy measurements at points (a) and (b) at each side of the northern canyon rim. The location of these points is shown in Fig. 8, using circles. Based on this comparison, we conclude that the present method is able to provide accurate predictions in nearshore/coastal areas characterised strongly 3D bathymetric features.

## CONCLUSIONS

The problem of transformation of the directional spectrum of an incident wave system over a region of strongly varying three-dimensional bottom topography is studied, in the context of linear theory. Bathymetric features are comparable in size with the dominant wave lengths and, thus, phase-average models are not expected to correctly predict the spatial distribution of the wave height and other useful quantities. The wave analysis has been performed using the Consistent Coupled-Mode Model (Athanassoulis and Belibassakis 1999, Belibassakis *et al* 2001) phase-resolving model. The linear transfer function, connecting the incident wave with the wave conditions at each point in the field is calculated. This model takes into account reflection, refraction and diffraction phenomena. The present approach permits the consistent transformation of the full incident directional wave spectrum over variable bathymetry regions and the calculation of the spatial evolution of point spectra of all interesting wave quantities (free surface elevation, velocity, pressure), at every point in the domain. Moreover, the present model can be extended to treat weakly non-linear waves, and it can be further elaborated for modeling and studying wave propagation over random bottom topography.

## ACKNOWLEDGMENTS

The present work has been partially supported by the EU in the framework of EESD ENVIWAVE project: “Development and application of validated geophysical ocean wave products from ENVISAT, ASAR and RA-2 instruments” (EVG1-CT-2001-00051). Also, the authors would like to acknowledge Thomas Herbers, Fabrice Ardhuin and Rudy Magne for fruitful discussions, collaboration and exchange of data and information from the NCEX, funded by ONR and NSF. Moreover, Kostas Belibassakis would like to thank Thomas Herbers for the invitation to visit Dept. of Oceanography, Naval Postgraduate School at Monterey, California and perform first wave analysis at NCEX site using CCMM.

## REFERENCES

- Ardhuin, F. and Herbers, T.H.C. (2002) “Bragg scattering of random surface gravity waves by irregular seabed topography”, *J. Fluid. Mech.*, 451, 1-33.
- Athanassoulis, G.A. and Belibassakis, K.A. (1999) “A consistent coupled-mode theory for the propagation of small-amplitude water waves over variable bathymetry regions”, *J. Fluid. Mech.*, 389, 275-301.
- Athanassoulis, G.A., Belibassakis, K.A., Georgiou Y. (2003) “Transformation of the Point Spectrum over Variable Bathymetry Regions”, *13<sup>th</sup> Intern. Offshore and Polar Conference and Exhibition, ISOPE2002*, Honolulu, Hawaii, USA.
- Balay, S. et al (2004) “PETSc Users Manual, ANL-95/11 - Revision 2.1.5”, Argonne National Laboratory.
- Belibassakis, K.A., Athanassoulis, G.A. and Gerostathis Th. (2001) “A coupled-mode model for the refraction-diffraction of linear waves over steep three-dimensional bathymetry”, *Applied Ocean Res.* 23(6), 319-336.
- Belibassakis, K.A. and Athanassoulis, G.A. (2002) “Extension of second-order Stokes theory to variable bathymetry”, *J. Fluid. Mech.*, 464, 35-80.
- Booij, N., Ris, R.C., and Holthuijsen, L.H., 1999, A third-generation wave model for coastal regions. 1. Model description and validation, *J. Geophys. Res.*, 104(C4), p. 7649-7666.
- Chamberlain, P.G. and Porter, D. (1995) “The modified mild-slope equation”, *J. Fluid. Mech.*, 291, 393-407.
- Demmel, J.W., Gilbert, J.R., Li, X.S., 1999 “An asynchronous parallel supernodal algorithm for sparse gaussian elimination” *SIAM J. Matrix Analysis and Applications* 20(4), 915-952.
- Donelan, M.A., Hamilton J., and W.H. Hui (1985) “Directional spectra of wind-generated waves”, *Phil. Trans. Roy. Soc.*, A315, 509-562.
- Goda, Y. (2000) *Random Seas and Design of Maritime Structures* (2<sup>nd</sup> Ed.), World Scientific.
- Holthuijsen, L.H., A. Herman and N. Booij (2003) “Phase-decoupled refraction-diffraction for spectral wave models”, *Coastal Engineering*, 49, 291-305
- Massel, S. (1993) “Extended refraction-diffraction equations for surface waves”, *Coastal Engng*, 19, 97-126.
- Massel, S. (1996), *Ocean Surface Waves: Their Physics and Prediction*, World Scientific.
- Pelinovsky, E., Razin, A.V. and Sasorova, E.V. (1998) “Berkhoff approximation in a problem on surface gravity wave propagation in a basin with bottom irregularities”, *Waves in Random Media*, 8(2), 255-268.
- Ris, R.C., Holthuijsen, L.H., and Booij, N., (1999) “A third-generation wave model for coastal regions. 2. Verification”, *J. Geophys. Res.*, 104(C4), p. 7667-7681.